Three-dimensional CFD simulation of two-phase flow and electric field in an alkaline electrolyzer

Jinhao Bai[1,2], Xiaoping Guan[1,2], Ning Yang[1,2*]

1 State Key Laboratory of Multiphase Complex Systems, Institute of Process Engineering, Chinese Academy of Sciences, P. O. Box 353, Beijing 100190, China

2 School of Chemical Engineering, University of Chinese Academy of Sciences, Beijing 100049, China

**Corresponding author: nyang@ipe.ac.cn (N. Yang)*

Highlights

- *Neglecting electrochemical reactions yielded lower gas void fraction than coupling.*
- *Void fraction distribution shifts from outlet accumulation to both sides.*
- *Higher liquid velocity correlates with increased gas production and current density.*

1. Introduction

Water electrolysis, powered by renewable energy sources, holds significant potential as a future green energy source owing to its cleanliness, safety, and absence of greenhouse gas emissions[1]. Alkaline water electrolysis technology, known for its low investment cost, compact equipment structure, and simple flow channel, has already achieved commercialization. The pressure-filtered electrolyzer is a commonly used alkaline electrolyzer, with the cell composed of multiple electrolytic units stacked in a regular pattern. Mastoid plates are widely employed in industry due to their ease of fabrication through punching, high anti-compression capability, and low flow losses.

Nevertheless, the characterization of the two-phase flow within the electrodes and the distribution of current density, both crucial for performance assessment, remains a challenging endeavor. Numerous researchers have explored the impact of arrangement and structural parameters of concave-convex units within mastoid plates on flow and heat transfer characteristics, employing either experimental methods or numerical simulations. However, the majority of studies have focused on a limited number of cylindrical or square structures, and there is a noticeable dearth of research on the flow characteristics within channels formed by a larger number of concave-convex units.

Recently, Wang et al. [2] conducted an investigation into single-phase flow on large-scale mastoid plates. Their findings revealed notable dead zones in the flow field on both sides of the bipolar plates, emphasizing poor fluid distribution uniformity within the plates. Additionally, Gao et al. [3] developed a three-dimensional numerical simulation of the electrolyzer using a coupled multiphase flow and electrochemical model. The results highlighted that a moderate increase in electrolyte concentration, flow rate, and spacing between conductive columns effectively reduced the cell voltage.

However, to the best of the authors' knowledge, no studies have reported on the multiphase flow characteristics and electrochemical performance within a large-scale mastoid plate electrolyzer. In this paper, we employed a three-dimensional Euler-Euler CFD simulation, coupled with an electric field model, to simulate the two-phase flow and the performance of the electrolyzer. The objective of this study is to gain a thorough understanding of the patterns of gas-liquid flow within the electrolyzer and provide guidance for practical industrial operations.

2. Numerical Methods

Governing equations

The conservation equations are governed by the two-fluid model. The general mass balance equation for gas phase is

$$\frac{\partial}{\partial t}\left(\alpha_g \rho_g\right) + \nabla \cdot \left(\alpha_g \rho_g \mathbf{u}_g\right) = \dot{m}_g \tag{1}$$

where ρ denotes the density of phase, α is the phase saturation, $\mathbf{u}$ denotes the flow velocity, $\dot{m}_g$ represents the volume-specific mass flow rate due to an electrochemical reaction, which is not zero only in the electrode cell.

Due to the continuous inflow and outflow of the alkaline solution, the reaction consumption in the liquid phase is neglected. The continuity equation for the liquid phase under this condition is expressed as follows

$$\frac{\partial}{\partial t}\left(\alpha_l \rho_l\right)+\nabla\cdot\left(\alpha_l \rho_l \mathbf{u}_l\right)=0 \tag{2}$$

The momentum conservation for phase i is modeled as

$$\frac{\partial}{\partial t}\left(\alpha_i \rho_i \mathbf{u}_i\right)+\nabla\cdot\left(\alpha_i \rho_i \mathbf{u}_i \mathbf{u}_i\right)=-\alpha_i \nabla P+\mathbf{F}_{\mathrm{D},i}+\nabla\cdot\left(\alpha_i \boldsymbol{\tau}_i\right) \tag{3}$$

where P denotes pressure, $\mathbf{F}_{\mathrm{D},i}$ represents the average drag force per unit volume, $\boldsymbol{\tau}_i$ is the viscous shear stress term in phase i, and can be expressed as

$$\boldsymbol{\tau}_i=\mu_i\left[\left(\nabla\mathbf{u}_i\right)+\left(\nabla\mathbf{u}_i\right)^{-1}\right]-\left(2/3\right)\mu_i\left(\nabla\cdot\mathbf{u}_i\right)\mathbf{I} \tag{4}$$

where $\mathbf{I}$ represents the unit tensor.

The flux of ion is modeled through Poisson's equation

$$\nabla\cdot\left(-k_{eff}\nabla\phi_e\right)=aJ_a \tag{5}$$

here k_{eff} is the effective ion conductivity. According to the Bruggeman equation, the electrolyte conductivity k_{eff} is related to the gas volume fraction and can be expressed as

$$k_{eff}=k_0\left(1-\alpha_g\right)^{1.5} \tag{6}$$

As oxygen is generated in the anode electrode, the reaction term can be written as

$$\dot{m}_g=a\frac{M_{\mathrm{O}_2}}{4F}J_a \tag{7}$$

where a is the specific surface area of the anode, J_a is represented by the Butler-Volmer equation

$$J_a=\alpha_l^{\,2}J_{a,0}\left[\exp\left(\frac{2\gamma F}{RT}\eta\right)-\exp\left(\frac{2(\gamma-1)F}{RT}\eta\right)\right] \tag{8}$$

where γ is the transfer coefficient, F and R denote the Faraday constant and the ideal gas constant, respectively. The term α_l^2 refers to the interfacial effect of bubble coverage on electrochemical current density[4]. η represents the activation overpotential, defined as

$$\eta=\phi_s-\phi_e-\phi_0 \tag{9}$$

where ϕ_0 is the equilibrium potential, ϕ_s is the electric potential, and due to significantly higher electron conductivity compared to ion conductivity, the voltage drop across electrons is neglected, making this value equivalent to the applied voltage.

Finally, the drag model, as presented by Schiller and Naumann [5], is formulated as follows

$$\mathbf{F}_{\mathrm{D},g}=-\mathbf{F}_{\mathrm{D},l}=\frac{3}{4}\alpha_g\alpha_l\rho_l\frac{C_{\mathrm{D}}}{d_{\mathrm{b}}}\left|\mathbf{u}_l-\mathbf{u}_g\right|\left(\mathbf{u}_l-\mathbf{u}_g\right) \tag{10}$$

Geometry and Boundary Conditions

The structures of the anode and cathode electrolyte chambers are identical. Therefore, this paper only simulates the two-phase flow characteristics within the anode chamber. The geometric structure is illustrated in Figure 1, with a uniform distribution of concave-convex units, including the alkali inlet,

the alkali channel formed between the concave-convex units and the wall, the electrode, and the alkali outlet. The alkali solution first enters the gap formed by the closely pressed nickel electrodes and the bipolar plates through radial pore channels. Subsequently, electrolytic reactions occur on the electrodes, leading to gas generation. Finally, the resulting gas-liquid mixture flows out from the top exit. The specific dimensions of the computational domain are presented in **Table 1**.

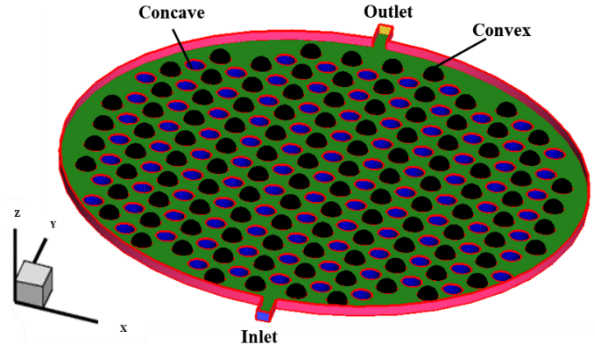

Figure 1: Schematic diagram of the computational domain: inlet and outlet channels, and convex-concave units.

Table 1. Computational domain structural parameters.

Parameters	Values
Width of inlet/outlet channel / mm	10
Height of inlet/outlet channel / mm	7.5
Depth of inlet/outlet channel / mm	20
Number of concave units	105
Number of convex units	112

The CFD simulation was conducted using the commercial CFD code Ansys Fluent. The electrochemical reaction source was integrated through user-defined functions (UDFs). A transport equation was formulated to solve the ion potential using the user-defined scalar (UDS). The first-order implicit scheme was employed to discretize the transient term, while the first-order upwind scheme was applied to the convective term. The phase-coupled SIMPLE approach was chosen to handle pressure-velocity decoupling. The time step was set at 0.0001 s.

The ion potential was set to zero on the anode side of the plate. A zero-flux boundary condition was applied to the ion potential on all other boundaries, as no ions are expected to pass through them. A mass flow rate boundary was prescribed at the channel inlet, while a pressure-outlet boundary condition with liquid backflow was set at the channel outlet, and the operating pressure was maintained at 1.6 MPa. A no-slip boundary was used for all wall surfaces.

3. Results and discussion

Model validation

Due to the current lack of experimental data on gas holdup in three-dimensional pressure-filter electrolyzers, a direct comparative analysis is not feasible. Therefore, we have chosen to validate the accuracy of the model by leveraging Riegel's data [5] data on hydrogen holdup from experiments conducted on a smaller scale, membrane-less electrolyzer. Figure 2 presents the hydrogen distribution profiles at a height of 12 cm with a current density of 6250 A/m^2. The simulated curve exhibits commendable agreement with the experimental data. It is worth noting that the simulated hydrogen holdup becomes slightly smaller than that observed in the experiment as the direction increases. This discrepancy may arise from simplifying the gas phase without accounting for the impact of water vapor evaporation.

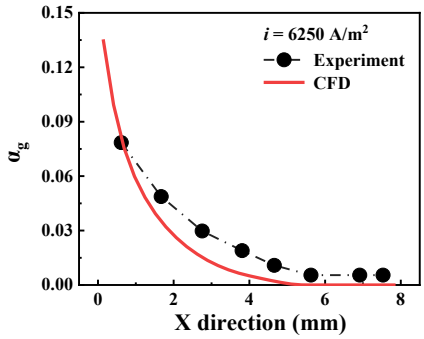

Figure 2: The comparison of experimental results and simulated hydrogen distribution profiles along the x-axis at y = 12 cm.

Influence of Electrochemistry

Figure 3 illustrates the variation in the overall gas holdup of the system when considering or neglecting electrochemical reactions. From the graph, it is evident that without considering electrochemical reactions, the system's gas holdup is lower. This difference is particularly pronounced at higher system gas holdup, reaching a maximum deviation of up to 10%. This difference originates from the inclusion of electrochemical reactions, introducing a non-uniform distribution of current density. The natural accumulation of gas in the flow direction results in a reduced gas holdup upstream, leading to elevated current density and increased gas production, as shown in Figure 4. In contrast to decoupled electrochemistry, this results in a prolonged residence time for the gas, ultimately contributing to a higher overall gas void fraction. Additionally, Figure 5 displays the radial gas distribution with and without electrochemical. It can be observed that the gas holdup is lower when electrochemical are not considered, consistent with Figure 3. However, the overall trend in both cases remains essentially the same. This suggests that the presence or absence of electrochemical does not markedly affect the characteristics of gas holdup distribution in the system.

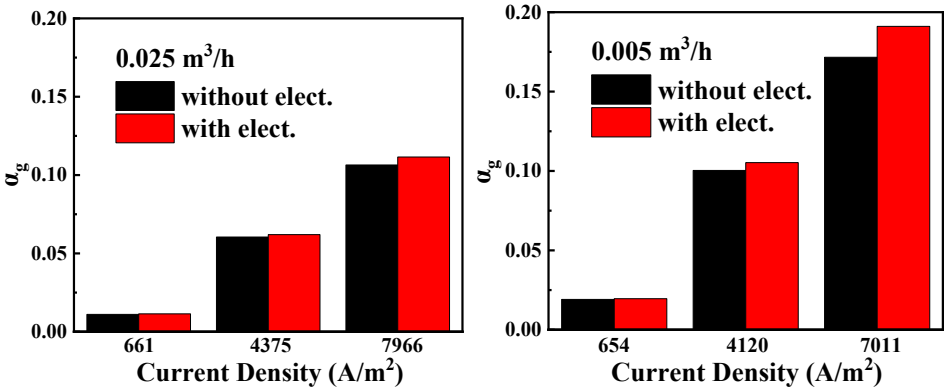

Figure 3: The overall gas holdup under varying current densities and liquid velocities with and without electrochemical.

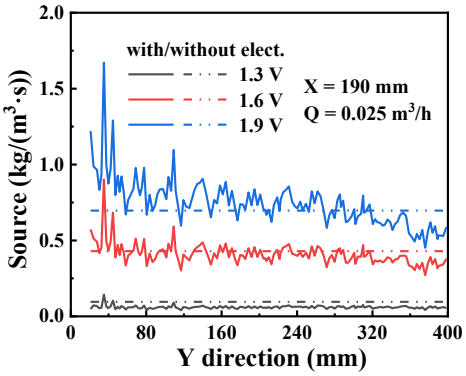

Figure 4: Distribution of electrode gas production along axial direction with and without electrochemical at various voltages.

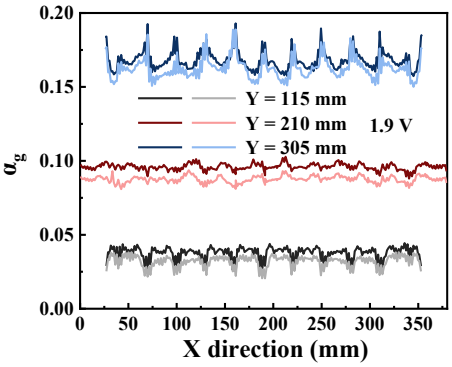

Figure 5: Radial gas holdup distribution at different heights with and without electrochemical at 1.9V.

Characteristics of Gas Holdup Distribution

Figure 6 illustrates gas production and electrode average current density at different voltages and liquid velocities. It can be observed that, at the same voltage, increasing the liquid velocity results in higher gas production and current density. This is attributed to higher liquid velocities, which reduce the system's gas holdup, decrease the reaction overpotential, and accelerate the reaction rate, consequently leading to increased gas production and current density.

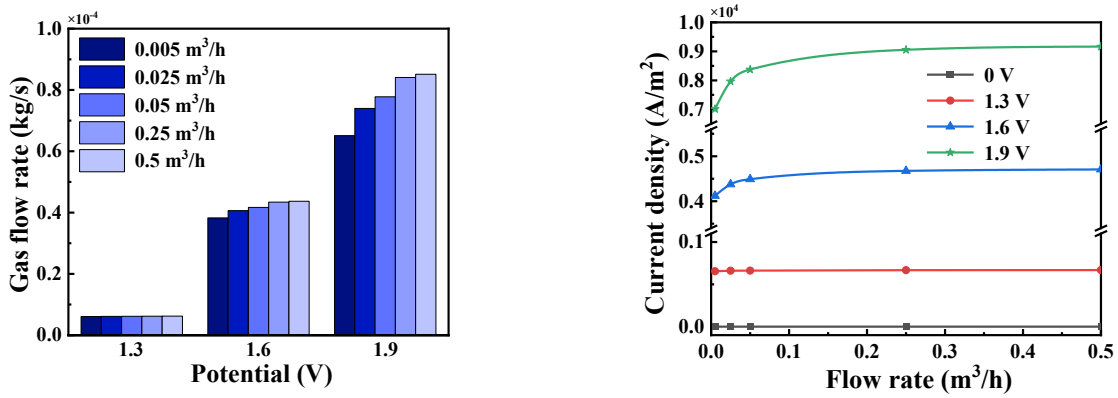

Figure 6: Gas production and electrode average current density at various voltages and liquid velocities.

Figure 7 presents the contour of gas holdup distribution under different operating conditions. It is evident that higher liquid velocities correspond to lower gas holdup, consistent with the trend observed in Figure 6. It is worth noting that, at lower liquid velocities, gas accumulates downstream, presenting a 'layered distribution' with lower concentrations upstream and higher concentrations downstream. As the liquid velocity increases, the gas accumulation transitions to the sides, forming a 'tree-like distribution' with higher concentrations on both sides and lower concentrations in the middle. The observed shift, marking a transformation in the flow pattern within the electrolyzer, is reported here for the first time.

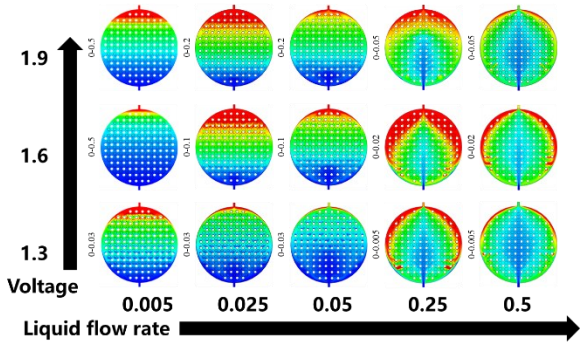

Figure 7: Cross-sectional gas holdup distribution contour at various voltages and liquid velocities.

4. Conclusions

We employed a Euler-Euler coupled electric field model to investigate the gas-liquid flow characteristics and electrolytic performance on the anode side of a three-dimensional large-scale mastoid plate electrolyzer. The following conclusions have been obtained:

1. Omitting electrochemical reactions resulted in a decrease in overall gas holdup compared to simulations incorporating electrochemistry.
2. Under identical voltage conditions, increasing liquid velocity correlated with higher gas production and increased current density.
3. At lower liquid velocities, gas accumulates downstream, transitioning from a ‘layered’ to a ‘tree-like’ distribution as velocity increases, signifying a shift in the electrolyzer's flow pattern.

These simulations provide valuable insights for formulating process intensification strategies, expediting gas removal, and refining the design and operation of electrolysis for optimization.

References

[1] Zhang X. The Development Trend of and Suggestions for China’s Hydrogen Energy Industry. Engineering. 2021;7(6):719-721.

[2] Wang T, Wang J, Wang P, Wang F, Liu L, Guo H. Non-uniform liquid flow distribution in an alkaline water electrolyzer with concave-convex bipolar plate (CCBP): A numerical study. Int. J. Hydrogen Energy. 2023;48(33):12200-12214.

[3] Gao L-Y, Yang L, Wang C-H, Shan G-X, Huo X-Y, Zhang M-F, Li W, Zhang J-LJJoE. Three-Dimensional Two-Phase CFD Simulation of Alkaline Electrolyzers. 2023;29(9):2207081.

[4] Schiller L, Naumann A. Fundamental calculations in gravitational processing. Zeitschrift Des Vereines Deutscher Ingenieure. 1933;77:318-320.

[5] Riegel H, Mitrovic J, Stephan K. Role of mass transfer on hydrogen evolution in aqueous media. J. Appl. Electrochem. JAN 1998;28(1):10-17.

Keywords

alkaline electrolyzer; convex-concave structure; electrochemistry; two-phase flow